A porosity-based flood inundation modelling approach for enabling faster large scale simulations

Advances in Water Resources 162 (2022) 104141

Contents lists available at ScienceDirect

Advances in Water Resources

journal homepage: www.elsevier.com/locate/advwatres

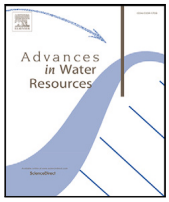

A porosity-based flood inundation modelling approach for enabling faster large scale simulations

Vita Ayoub [a,b,c,*], Carole Delenne [b,c], Marco Chini [a], Pascal Finaud-Guyot [b,c], David Mason [d], Patrick Matgen [a], Ramona Maria-Pelich [a], Renaud Hostache [a,e]

[a] Luxembourg Institute of Science and Technology, Environmental Research and Innovation Department, Esch-sur-Alzette, Luxembourg
[b] HSM, Univ. Montpellier, CNRS, IRD, Montpellier, France
[c] Inria, Team Lemon, Montpellier, France
[d] University of Reading, Department of Geography and Environmental Science, Reading, United Kingdom
[e] UMR Espace-Dev, IRD, Univ. Réunion, Univ. Guyane, Univ. Antilles, Univ. Nouvelle Calédonie, UPVD, Univ. Montpellier, Montpellier, France

ARTICLE INFO

Keywords:
Shallow water model
Porosity-based model
Flood inundation
Large scale
High-resolution data
Fast simulations

ABSTRACT

Floods are among the most devastating natural hazards in the world. With climate change and growing urbanisation, floods are expected to become more frequent and severe in the future. Hydrodynamic models are powerful tools for flood hazard assessment but face numerous challenges, especially when operating at a large scale. The downside of discretising an area using a fine mesh yielding more accurate results, is the expensive computational cost of simulations. Moreover, critical input information such as bathymetry (i.e, riverbed geometry) are required but cannot be easily collected by field measurements or remote sensing observations. During the past few years, the development of sub grid models has gained a growing interest as these enable faster simulations by using coarser cells and, at the same time, preserve small-scale topography variations within the cell. In this study, we propose and evaluate a modelling framework based on the shallow water 2D model with depth-dependent porosity enabling to represent floodplain and riverbed topography through porosity functions. To enable a careful and meaningful evaluation of the model, we set up a 2D classical model and use it as a benchmark. We also exploit ground truth data and remote sensing derived flood inundation maps to evaluate the proposed modelling framework and use as test cases the 2007 and 2012 flood events of the river Severn. Our empirical results demonstrate a high performance and low computational cost of the proposed model for fast flood simulations at a large scale.

1. Introduction

With the increasing risk of more frequent and severe floods (Arnell and Gosling, 2016) due to climate change and growing urbanisation, there is a crucial need to make more investments in flood management. Impacts of floods include human, socio-economical and environmental losses. Poorly conducted hazard assessments can lead to inefficient risk management, from insufficient protective mitigation measures to expensive rebuilding of devastated areas (Baan and Klijn, 2004; Meyer et al., 2009). Instead, well-conducted flood risk assessments provide a valuable support for decision making related to urban planning and emergency response preparedness. Therefore, it is essential to improve flood management systems to better anticipate and further reduce potential flood risk (Pradhan et al., 2014; Tehrany et al., 2014). In this context, hydrological and hydraulic models play a central role in flood forecasting as they provide predictions of water streamflows and levels across various temporal and spatial scales (Revilla-Romero et al., 2016; Hostache et al., 2018).

The most common flood inundation (hydraulic) models are based on the depth-averaged Navier Stokes equations, also called de Saint-Venant or Shallow Water Equations (SWE). The resolution of these equations can be carried out in one (1D) or two dimensions (2D). 1D models solve the 1D formulation of the SWE (Bates and De Roo, 2000) where the flow is assumed to be unidirectional and water levels are assumed to be constant across sections. Although they are relatively easy to setup and fast to run (Cunge, 1980), these models fail to provide accurate predictions of overbanking flow and in presence of complex topographies, especially because the momentum transfers between the channel and the floodplain are neglected. 1D-storage area models (also often referred to as 1D+ or quasi-2D) are sometimes preferred as they

* Corresponding author at: Luxembourg Institute of Science and Technology, Environmental Research and Innovation Department, Esch-sur-Alzette, Luxembourg.
E-mail address: vitaayoub@outlook.com (V. Ayoub).

https://doi.org/10.1016/j.advwatres.2022.104141
Received 20 July 2021; Received in revised form 19 January 2022; Accepted 24 January 2022
Available online 9 February 2022

include a representation of floodplain storage using a series of user-defined polygonal compartments into which overbank flows can spill. The flow between the main channel and the floodplain storage cells is modelled using stage-discharge equations, such as weir, gate or orifice laws. These can also be used to link storage cells to one another, and the water level is then computed using volume conservation in each storage cell. However, these models also neglect the momentum conservation between storage areas in floodplains. To tackle the previously described issues, 2D approaches are adopted. In 2D flood modelling, a fine discretisation of the area of interest (including main channel and floodplains) is required to accurately represent topography. Consequently, the main limitation of accurate modelling of large scale floods is associated with a very expensive computational cost. An alternative approach relies on the coupling of 1D and 2D models. This approach is not completely satisfying as it only accounts for mass transfers between the two models. The actual key for this approach to be reliable is correctly representing edges of the 1D and 2D models making it possible to keep the spatial and temporal correlations of 1D and 2D models consistent (Zhang et al., 2020). For instance, Willems et al. (2002) represents the floodplain by fictitious river-branches for which the calibration of friction coefficients is required to account for momentum. A precise mapping of these branches is necessary to accurately delineate the flood extent that is otherwise often overestimated. Finaud-Guyot et al. (2011) proposed a shallow water based model for river-floodplain interactions using 1D and 2D elements in the main channel and floodplain, respectively. This allowed to improve the portraying head loss phenomena that can happen due to channel bends or meander shortcuts, thanks to the inclusion of lateral momentum transfer between the river and the floodplain.

To correctly capture flood dynamics there is a need to further reduce the computational time while ensuring precise representation of river-floodplain connections. Sub-grid modelling approaches have tackled this challenge and gained a growing interest as they are a good compromise between accuracy and high computational efficiency. Indeed, they enable faster simulations as they use coarser computation cells while accounting for small-scale topography variations within the cells. For example, Lisflood-FP is a fast-running and relatively easy-to-set-up model and its standard version was introduced by Bates and De Roo (2000). It was further developed by Neal et al. (2012) who proposed a version enabling subgrid capability in the channel. This assumes a simplified channel shape and uses a 1D approach for the channel flow simulation and a 2D approach for the floodplain. The adopted subgrid channel approach allows representing any river channel size, even below the grid resolution. However, the subgrid approach only applies to the river and the resolution in the floodplain has to be rather high to accurately represent floodplain flows and inundation extent.

Other modelling techniques rely on two dimensional shallow water models including the porosity concept as a way to upscale the traditional shallow water equations. Porosity is defined as the fraction of a computational cell/edge available to the flow. Porosity-based models have evolved over the past twenty years. First, Defina et al. (1994) introduces the shallow water model with isotropic porosity. The formulation for partially wet/dry areas over irregular domains is later improved by Defina (2000), Casulli (2015) and Hervouet et al. (2002). In the single porosity model (Guinot and Soares-Frazão, 2006) a differential formulation is derived using a finite volume scheme, which is further evaluated by Soares-Frazão et al. (2008). Later, Sanders et al. (2008) shifts the focus from isotropic to anisotropic porosity by proposing the Integral Porosity model, where connective porosity (through edges) is distinguished from storage porosity (within cells). Guinot (2012) then merges the isotropic and anisotropic models and introduces a multiple porosity approach for applications in urban areas. Kim et al. (2015) investigates the porosity-based model errors and show that they are lower for anisotropic models than for isotropic approaches. This approach is further extended by introducing a Dual Integral Porosity (DIP) model (Guinot et al., 2017). The SW2D-DDP model was presented and evaluated in Guinot et al. (2018). In this article, synthetic test cases (a series of dam-break configurations and a meandering channel) and an experimental test case were used to evaluate and validate the model results. Two closure laws (Integral Porosity and the depth-dependent Dual Integral Porosity) were compared to a fine 2D model that solves the classical shallow water equations with the second-order MUSCL-EVR scheme. Results show the superiority of the proposed DIP closure model on the IP model. Moreover, the paper presented a shallow water model based on the DIP approach, with depth-variable porosity fields: SW2D-DDP, and it has been found that although porosity approach cannot represent details within the cells, it shows good agreement with the average values of the fine 2D model. Moreover, the CPU ratio between DDP and fine 2D models ranges from 310 to 2900. In this paper, we apply and validate the SW2D-DDP model on a real large scale test case, since it was already evaluated on synthetic test cases in Guinot et al. (2018).

The provision of accurate bathymetric data is critical in hydrodynamic modelling, yet obtaining this information where in situ measurements are lacking is not always possible. In this context, Hostache et al. (2015) proposes a method for retrieving effective riverbed bathymetry based on the assimilation of water level measurements acquired by a drifting GPS buoy into a 1D hydraulic model and many bathymetry retrieval methods have been recently developed in the framework of SWOT satellite mission preparation (e.g. Oubanas et al. (2018), Yoon et al. (2012), Durand et al. (2014)). In the perspective of retrieving bathymetry that is often unknown (Larnier et al., 2021; Delenne et al., 2021), we propose here to represent it via depth-dependent porosity functions. We therefore hypothesise that bathymetry can be effectively represented through depth-dependent porosity parameters.

In this context, the main objective of this study is to develop and evaluate a modelling framework based on SW2D-DDP enabling fast flood inundation simulations at a large scale, while representing for the first time both bathymetry and small-scale floodplain topography using depth-dependent porosity within comparatively large computational cells. To evaluate the proposed modelling framework with scrutiny, we compare the SW2D-DDP simulation result with a standard 2D shallow water model on one hand. Moreover, we evaluate both model results using ground truth data (in situ measured and remote sensing-derived). Benchmarking the SW2D-DDP model against a high-resolution 2D model enables the evaluation of our approach across space and time. It also helps to explore strengths and limitations of the proposed approach in comparison with state of the art approaches. Our study site is a 1500 km^2 floodplain located at the confluence of the Severn and Avon rivers in the United Kingdom, which has frequently experienced flooding especially in the last decades. The 2007 and 2012 flood events are used as test cases.

The remainder of this paper is organised as follows. In Section 2, we present the proposed modelling framework enabling the simplified representation of bathymetry and topography via porosity, and then the design of the experiment to evaluate the model performance. Next, the study site and available data, as well as the models set up are described in Section 3. In Section 4, we evaluate the simulated flood extent and water level maps. Finally, Section 5 discusses the main outcomes of the study.

2. Methodology and experimental setup

This section first describes the proposed modelling approach based on the shallow water 2D model with SW2D-DDP. Next, it presents the experimental setup for evaluating the model performance using a standard 2D shallow water (SW2D) model as a reference, as well as in situ measured and remote sensing-derived data.

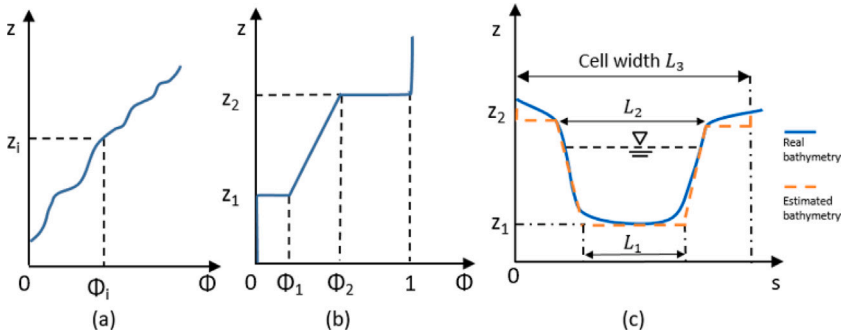

Fig. 1. Porosity laws: (a) law type 0; (b) law type 3; (c) bathymetry representation using law type 3. z: elevation, ϕ: porosity, s: abscissa along the river cross-section.

2.1. Modelling framework

SW2D[1] is a modelling suite that has been progressively developed and further improved since 2002. It solves the 2D shallow water equations with a finite volume scheme on structured or unstructured grids. The SW2D-DDP model (Guinot et al., 2018), introduces a Depth-Dependent Porosity that accounts for small-scale effects of obstacles to the flow in a macroscopic way without the need to detail their geometry in the mesh. Although the whole domain is represented as flat in the mesh, a bottom elevation z_b is provided inside each cell via a porosity distribution as a function of the water depth.

Within a domain $\mathcal{D}$, the model distinguishes storage (cell) porosity ϕ_Ω from edge (connective) porosity ϕ_Γ. The storage porosity for a given cell is the adimensional area available for water at the elevation z_s. As detailed in Guinot et al. (2018), the standard shallow water equations are multiplied by the phase function ϵ, defined as:

$$\epsilon(x,y,z) = 1 \text{ if } z > z_b, 0 \text{ otherwise} \tag{1}$$

where $\epsilon(x,y,z)$ is the phase indicator for the point coordinates (x,y,z) that is equal to 0 if the point is in the solid phase (i.e. lower than the bottom elevation z_b). The porosities represent the amount of water that can be stored per unit domain and boundary for a unit variation in the free surface elevation $z_s(x,y)$, which is assumed to be known. Thus, the porosities over cells (Ω) and edges (Γ) are defined as:

$$\phi_D(z) = \frac{1}{D}\int_D \epsilon(x,y,z)\,\mathrm{d}D, \quad \mathcal{D} = \Omega, \Gamma \tag{2}$$

where $\mathcal{D}$ stands for either a cell (Ω) or an edge (Γ). This allows to uniquely define the volume of water stored per unit area/length in the sub-domain $\mathcal{D}$ between the ground and the elevation z as:

$$\theta_D(z) = \int_{-\infty}^{z} \phi_D(\zeta)\,\mathrm{d}\zeta \tag{3}$$

Small scale topography information is therefore taken into account via porosity laws Guinot et al. (2018). In the SW2D-DDP software, four law types are proposed. In this model setup, we have chosen to use only two types of porosity law (0 and 3) for the sake of simplicity and in order to show how porosity represents and preserves high resolution topographic data.

Law 0 is used for defining storage porosity in the floodplain (Fig. 1). The distribution of ground elevations $z_b(x,y)$ within each cell is first retrieved from the digital elevation model (DEM). Next, it is discretised using a piecewise constant function of N segments with "equidistant" porosity values associated to elevation values with the following relation:

$$\phi(z_i) = i/N, i = 1 \ldots N \tag{4}$$

where z_i is the subgrid water depth associated to a porosity ϕ_i and N is the number of segments.

[1] https://SW2D.inria.fr/.

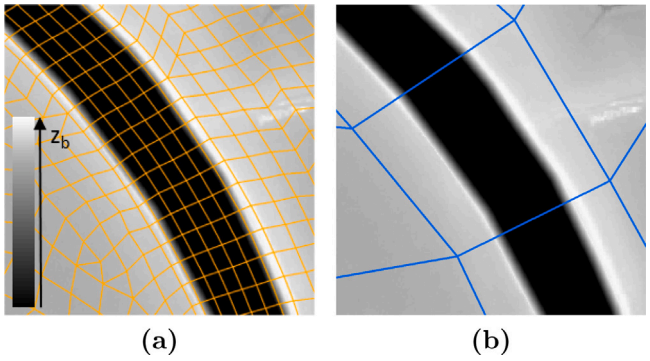

Fig. 2. 0.25 km^2 subset of: (a) the standard model mesh, (b) the porosity model mesh.

Law type 3 allows us to handle porosities inside riverbed cells. In line with the objective of minimising the number of cells in the model mesh and therefore reducing computational time, we propose to define cells with dimensions larger than the riverbed width. Moreover, to avoid elongated cells that can be responsible for model instabilities, we maintain the length of the computational cells along the streamflow direction at maximum twice its width (Fig. 2). Since bathymetric data is rarely available, we propose to represent riverbed geometry using a simplified trapezoidal shape assumption via the porosity law type 3 (Fig. 1).

First, storage porosities are computed. Then, the porosity law type used for the edges is selected depending on the location of their adjacent cells: law type 3 is used inside the riverbed (cross sections, i.e. edges between two cells of type 3) and law type 0 is used in the floodplain (between two cells of type 0) and on river banks (between a riverbed and a floodplain cells). To accurately represent overbank flows, the nodes of the river bed cells are positioned on the dikes in both models. Indeed, when positioning interfaces upon constrictions and obstacles, these latter are implicitly considered in the interface flux calculation, while the same obstacles disappear from the numerical representation when they are located inside the cells. Moreover, to ensure that high points are correctly taken into account without too much overloading the mesh design process, we choose to automatically compute the edge porosity values as the minimum of the porosities of their neighbouring cells. It is worth mentioning that the parameter retrieval of the porosity law in each cell and edge is carried out automatically using the available DEM and bathymetric information.

2.2. Experimental design

To the best of our knowledge, our modelling framework enables for the first time to represent both riverbed and floodplain subgrid topography using porosity laws. To evaluate its advantages and limitations, we compare the SW2D-DDP model with a standard fine 2D

model, namely SW2D (Inria Lemon Team, 2022), in terms of simulated water depths and inundation extents. Moreover, to further assess our modelling approach, we evaluate it against observed flood extents from aerial photographs and satellite images, and against observed water level time series from in situ measurements when available.

2.2.1. The standard 2D shallow water model

To enable a meaningful comparison between the two approaches, the standard model has to use exactly the same input data as the porosity model: topography, bathymetry, boundary and initial conditions and parameters (e.g. friction coefficient, numerical scheme). The two models differ only in the way they represent the floodplain and riverbed topography. The standard model being based on a classical finite volume scheme, the bottom elevation inside a computational cell has a unique value, equal to the average elevation of the cell's nodes. As a consequence, topography can be smoothed out within each cell, when flow obstructions, drains or structures (e.g. dikes, roads, streams) are not intrinsically represented via cells smaller than their dimensions. Indeed, adequately representing dikes, drains or river channels, requires to include several mesh cells within each of these structuring elements. Therefore, in the standard SW2D model, the mesh needs to be designed in a way that entire cells are placed explicitly on hydraulic structures or singularities. For instance when representing a drain of 5 m width, cells have to be well-placed to capture its effect, otherwise it would be transparent for the model. Having many of these structures in large scale areas would require a long time to represent them in a standard SW2D model.

2.2.2. Evaluation method

To evaluate the porosity model performance, we propose an approach composed of several successive steps detailed in the following paragraphs: (i) post-process model results to derive flood extent and water depth maps in the same format, (ii) compare flood extent and water level maps extracted from both models, on a daily basis; (iii) evaluate flood maps extracted from both models using remote sensing derived data; and (iv) evaluate simulated water level time series against in situ observation data. In this study we chose to evaluate the proposed modelling approach in terms of simulated water levels first using punctual in situ water level measurements. Next, as spatially distributed water level cannot be derived from in situ observation, we also compare the SW2D-DDP results with those obtained using the standard SW2D model. Whether we use the SW2D model results or the measurements provided by a camera or a gauging station to evaluate water levels, we computed the root mean squared deviations (RMSD, Eq. (7)). When we evaluate the model in terms of flood extents, two types of references are used : (i) the flood extent maps simulated by SW2D and (ii) the ones derived from a satellite imagery.

Post-processing of model results:. We aim to compare the results of the porosity and the reference models in terms of flood extents and water levels. By definition, the bottom elevation of the cells in the porosity and standard model meshes are taken into account differently. In the standard SW2D model, as previously mentioned, the bottom elevation of a cell corresponds to the average elevation of its nodes. In the porosity model, the subgrid elevation variability is accounted for via the porosity. Since the edges of the fine and coarse grid cells do not overlay, the flood extent maps derived from the two models are resampled to the original DEM resolution (2 m), to enable a pixel-to-pixel comparison. To do so, the cell is considered flooded when the simulated water depth reaches a minimum value $h_{\min}$ i.e. when $z_s > z_b + h_{\min}$ where z_b is the cell bottom elevation for the standard model and the DEM elevation for the porosity model. The $h_{\min}$ is set to 0.1 m, which corresponds approximately to the vertical accuracy of the LiDAR DEM.

Evaluation of simulated flood extent maps:. The simulated flood extents evaluation is carried out twice, using as a reference either (i) the standard model or (ii) the available Earth Observation data. Based on a pixel-by-pixel comparison, we compute a confusion matrix composed of four metrics: (1) the number of pixels that are unflooded in both maps, i.e. TN: true negatives, (2) the number of pixels flooded only in the standard model, i.e. FN: false negatives, (3) the number of pixels flooded only in the porosity (SW2D-DDP) model, i.e. FP: false positives, and (4) the number of pixels flooded in both maps, i.e. TP: true positives. To compare the simulated and the reference maps, we compute contingency maps. As overall performance metrics we use the Critical Success Index (CSI) (Schaefer, 1990) and the Overall Accuracy (OA) that are both derived from the confusion matrix. CSI and OA quantify the goodness of fit between the evaluated map and the reference maps (see Eqs. (5) and (6)). The CSI represents the ratio of the number of pixels correctly predicted as flooded (TP) over the number of all flooded pixels:

$$\mathrm{CSI} = \frac{\mathrm{TP}}{\mathrm{TP} + \mathrm{FP} + \mathrm{FN}} \tag{5}$$

The OA takes into account the agreement of non flooded areas and is defined as follows:

$$\mathrm{OA} = \frac{\mathrm{TP} + \mathrm{TN}}{\mathrm{TP} + \mathrm{FP} + \mathrm{FN} + \mathrm{TN}} \tag{6}$$

These scores vary between 0 and 1, with the highest value attained when the predictions present a perfect fit with the reference.

Evaluation of simulated water level maps:. To quantitatively measure discrepancies between the simulations and reference water level maps, we use the root mean square deviations (RMSD, Eq. (7)) between the porosity model predicted water levels $z_{i,\mathrm{sim}}$ and the reference water levels $z_{i,\mathrm{ref}}$ (Eq. (7)), resampled at the DEM resolution (2 m), and for each of the n inundated pixels of the entire domain.

$$\mathrm{RMSD} = \sqrt{\frac{1}{n}\sum_{i=1}^{n}\left(z_{i,\mathrm{sim}} - z_{i,\mathrm{ref}}\right)^2} \tag{7}$$

Moreover, to further evaluate the distribution of the differences between the simulated and reference water levels, we make use of boxplots showing the deviation distribution based on statistical metrics: (1) the lower bound; (2) the first quartile, Q1=25th percentile; (3) the median, Q2=50th percentile; (4) the third quartile, Q3=75th percentile and (5) the upper bound. The interquartile range (IQR) goes from the 25th to the 75th percentile, and therefore represents 50% of the data values. The maximum value of the boxplot is defined as Q3 + 1.5*IQR, and the minimum value Q1 −1.5*IQR. Outlier points are thus eliminated from the plot for the sake of readability.

Evaluation of simulated water levels time series:. Water level time series obtained from each of the porosity and standard models are evaluated against in situ observation data. For visual comparison, these time series are plotted. Then, to quantitatively measure the discrepancies, we compute the root mean square deviations (RMSDs), as described in the previous section.

3. Study area, experimental data and model setup

The Severn, the longest river in Great Britain, extends from its source at Plynlimon in the Welsh hills to the mouth of the Bristol channel. The overall catchment area covers approximately 11,000 km^2 and is predominantly rural, apart from some urban settlements like Worcester, Tewkesbury and Evesham. Fig. 3 shows the model domain and river network with the location of the available gauging stations and the camera location offering live imagery on the river Severn. The study site is located at the confluence of rivers Severn and Avon around the city of Tewkesbury and has been subject to frequent flooding due to intense precipitation. The area of interest covers approximately 15×10 km^2. Two flood events of different magnitude will be simulated and analysed to better understand the model behaviour with changes in boundary conditions: the July 2007 and November 2012 flood events.

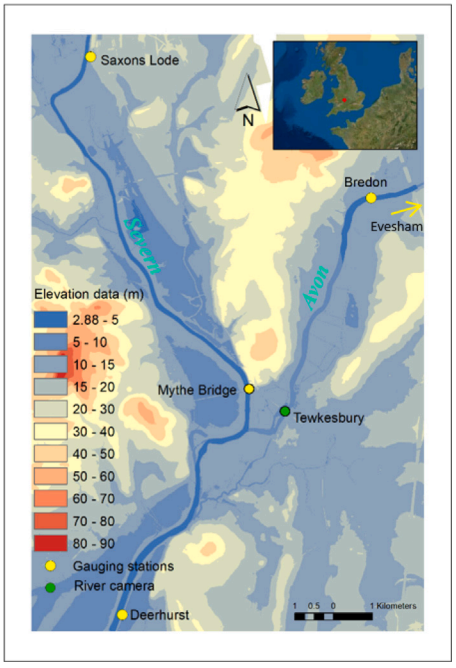

Fig. 3. Study site: model boundaries and location of the gauging stations and the river camera. The background colours illustrate the classification of ground elevation. (For interpretation of the references to colour in this figure legend, the reader is referred to the web version of this article.)

Hydrometric data:. Two suitable gauging stations are located at Saxons Lode (along the Severn River) and Evesham (along the Avon River) upstream of the confluence. Due to the backwater effect observed at Bredon, the streamflow time series is estimated there from that recorded at Evesham gauging station (located upstream of Bredon) and delayed in time based on an estimated wave travel time. Mythe Bridge is situated upstream the confluence of the Severn-Avon rivers and Deerhurst is situated downstream. Hydrometric data are provided by the UK Environmental Agency (EA) at 15 min-intervals. Moreover, the Tewkesbury stationary camera (Fig. 3) mounted on the wall of a building in March 2011, provided a view on the Avon river, which allowed taking hourly daylight images during the 2012 flood event. This camera enabled the estimation of water levels in the river (Vetra-Carvalho et al., 2020), which are used to evaluate the hydraulic model performance inside the domain.

Earth observation data:. The flood event of July 2007 is particularly interesting because an airborne campaign imaged the flood at a very high resolution (50 cm) on July 24, close to the flood peak (Giustarini et al., 2012). Flood extents were manually digitised on this imagery. This extracted flood map allows evaluating the simulated flood extents at the same date (24 July). The hierarchical split-based approach proposed by Chini et al. (2017) is used to derive flood extent maps from the Cosmos-SkyMed images acquired on the following dates: 27, 28, 29, 30 November and 01, 02, 04 December 2012. These flood maps are considered for evaluating synchronous flood extent maps simulated by the porosity and the standard models.

Topographic and bathymetric data:. A LiDAR DEM at 2m-spatial resolution with a vertical accuracy of 0.10 m provided by the UK Environmental Agency (EA) (Wood et al., 2016) is used to provide the model with ground elevation. Bathymetric data is reconstructed using three river cross section measurements at the upstream (Saxons Lode and Bredon) and downstream (Deerhurst) boundaries of the model. To do so, first, we approximate the observed cross sections using a trapezoidal shape. The bank lines are manually digitised along the Avon and Severn river streams and river stream bottom lines are automatically generated as parallels to the bank lines (using a distance estimated based on the observed cross sections). Next, the bank elevations are estimated by extracting ground elevation (provided by the Lidar DEM) along the bank lines. Then, the river bottom elevation is linearly interpolated between the three trapezoidal cross sections along the Avon and Severn bottom lines. Based on the river banks and bottom lines (with associated elevation values) we interpolate river bathymetry. Finally, the interpolated bathymetric data is merged with topographic data to form a single model input.

3.1. Model setup

While the standard model mesh is composed of 29,772 cells, the porosity model mesh contains only 1042 cells. Concerning the mesh design in the SW2D-DDP model, just like in any other hydraulic model, the cell including the river should not be too large as the porosity law used in river cells considers the flood plain as horizontal (rectangular above trapezoidal shape). For other cells, no brutal variations in terms of surface should be found between adjacent cells. The influence of the number of tabulations N inside a cell has been investigated in Guinot et al. (2018). Since the spatial information is lost within a coarse grid cell, it is essential to ensure that obstacles are captured by the 5 tabulation levels.

Discharge time series are imposed as upstream boundary conditions of the hydraulic model (Severn at Saxons Lode and Avon at Bredon). The streamflow time series in Saxons Lode are derived from water surface elevation records using a rating curve. Water level time series are used as downstream boundary condition at Deerhurst (Fig. 4). The initial condition is a fixed water level equal to the downstream condition. A uniform Strickler coefficient $K_s = 50\ \mathrm{m}^{1/3}\ \mathrm{s}^{-1}$ is used for the riverbed and the floodplain. Spatially distributed parameters could easily be prescribed but a sensitivity analysis (not shown in this paper) showed that the influence of the friction coefficient was limited for the studied flood event. The durations of 2007 and 2012 flood event simulations are 17 days (18 July–04 August) and 15 days (21 November–06 December), respectively.

4. Results

4.1. Evaluation of simulated flood extent maps

Fig. 5 shows the CSI and OA time series computed on a daily frequency for evaluating the SW2D-DDP simulated flood maps using the SW2D simulated flood maps as reference. It can be seen that both simulated flood extent maps are most of the time in agreement for both flood events. At the flood peak, in Figs. 6b and 7b, there is a very good agreement between the two models (accuracy of 95%). The model agreement is slightly lower in the rising limb, and decreases more in the falling limb. This implies that the draining dynamic in the SW2D-DDP model is different from that in the SW2D model. Figs. 6 and 7 show a series of contingency maps obtained by comparing the simulated flood extent maps (by the SW2D-DDP and SW2D models) during the 2007 and 2012 flood events. During the rising limbs (Figs. 6a and 7a) the porosity model exhibits a good agreement with the standard model, while locally inundating slightly larger areas especially in the upstream part as well as in little drains in the urban zone, at the Severn-Avon confluence (see box in Fig. 6a). This indicates the porosity model induces overbanking earlier than the standard model. Oppositely, a smaller inundation extent is visible locally nearby the Avon river. Figs 6c and 7c show a substantially larger flood extent simulated by SW2D. This indicates that almost all floodplain water came back to the stream in the SW2D-DDP simulation while a substantial volume of water remains present in the floodplain in the SW2D simulation. This effect is dominant in the eastern Severn floodplain and around the urban settlements. Overall, Figs. 6c and 7c suggest that the porosity

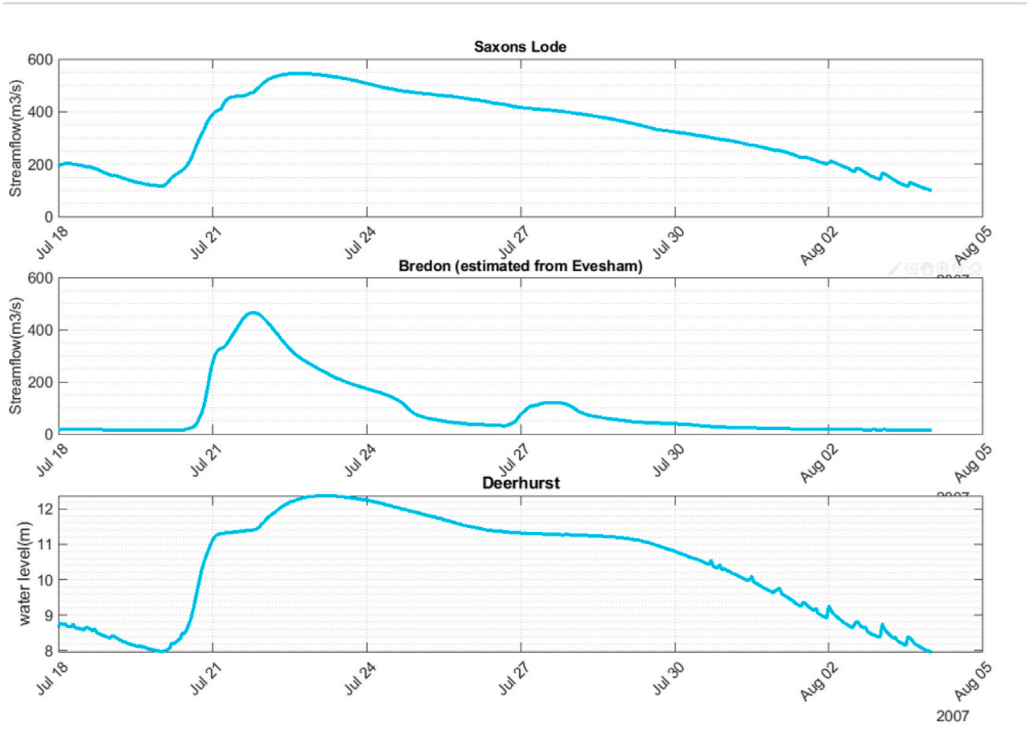

(a)

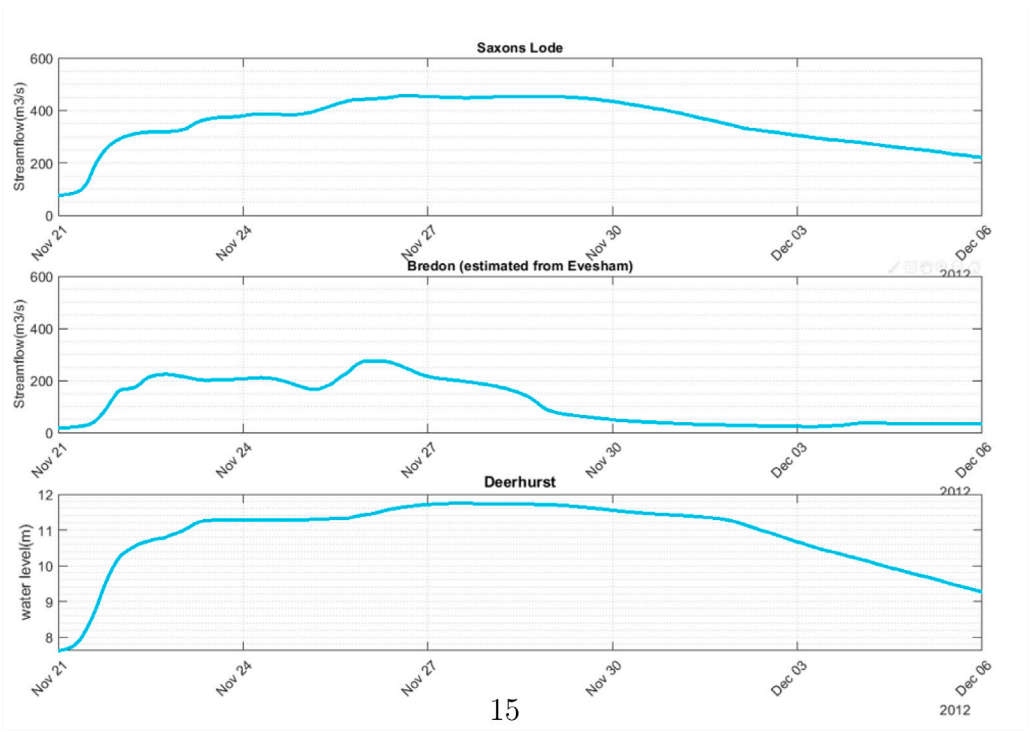

(b)

Fig. 4. Model boundary conditions for the 2007 (a) and the 2012 (b) flood events: Upstream streamflow (Saxons Lode and Bredon) and downstream water level (Deerhurst) time series.

model fills in and drains floodplain water faster than the standard model. To better understand and assess this aspect, we also compare both model results to remote-sensing derived data.

For the 2007 event, the porosity and standard model-derived flood maps were evaluated against the flood map extracted from aerial photography, and showed similar levels of agreement (CSI=0.92; OA=0.95 and CSI=0.9; OA=0.94 respectively for SW2D-DDP and SW2D). During the 2012 flood simulation, both models are in good agreement, with lower scores for the last satellite image (04 December, see Table 1). CSI and OA are rather similar for the two models but it is worth highlighting that the metrics of the porosity model are always exceeding those of the standard model. Fig. 8 shows the contingency maps computed

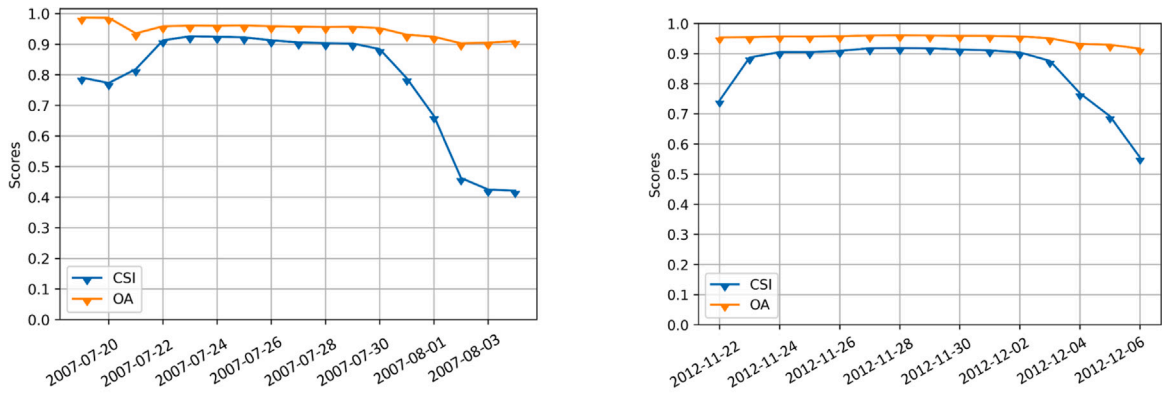

(a) 2007 (b) 2012

Fig. 5. CSI and OA scores time series showing agreement between simulated (porosity) and "reference" (standard) flood extent maps, CSI: Critical Success Index & OA: Overall Accuracy.

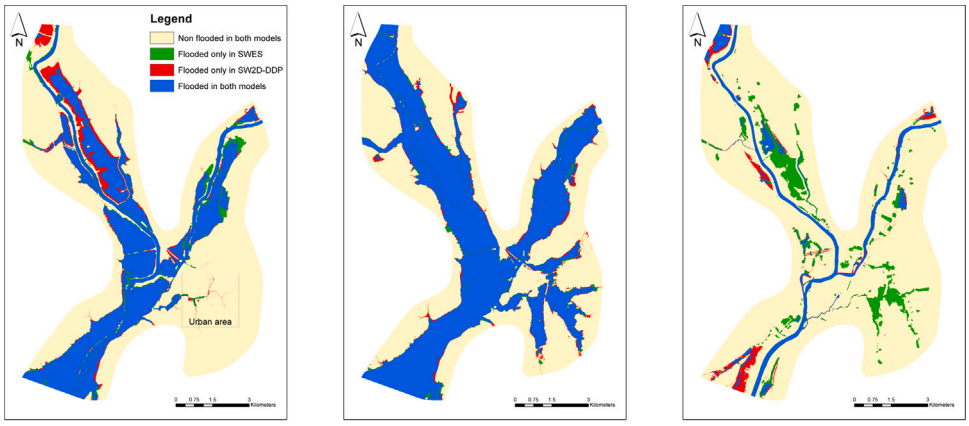

(a) Day 3 - 2007 (b) Day 7 - 2007 (c) Day 16 - 2007

Fig. 6. Contingency maps between porosity and fine models for simulation days 3, 7 and 16 of the 2007 flood event.

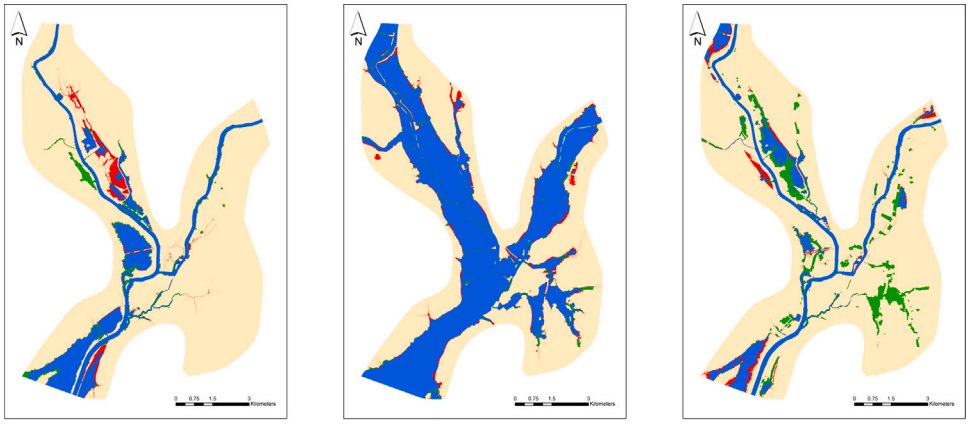

(a) Day 1 - 2012 (b) Day 5 - 2012 (c) Day 15 - 2012

Fig. 7. Contingency maps between porosity and fine models for simulation days 1, 7 and 15 of the 2012 flood event.

by each of the models using as a reference the satellite flood map acquired on December 04. The most important differences between the two simulated flood extent maps are exhibited close to Tewkesbury where SW2D-DDP drains water faster than SW2D. The flood extent map derived from SW2D therefore exhibit in Fig. 8a a substantial overestimation when compared to the flood extent map derived from a Cosmo-SkyMed image. However, this overestimation has to be interpreted carefully as SAR backscatter images do not enable floodwater detection in dense urban areas (Chini et al., 2019). Moreover, Giustarini et al. (2012) showed for the same study area that part of the floodwater

Table 1
Performance of the flood inundation extents simulated by the porosity (SW2D-DDP) and standard (SW2D) models computed using as a reference the satellite flood extent maps available for the 2007 and 2012 events. CSI: Critical Success Index; OA: Overall Accuracy.

Year	2007	2012						
Day	25–07	27–11	28–11	29–11	30–11	01–12	02–12	04–12
CSI (SW2D)	0.9	0.691	0.677	0.687	0.649	0.658	0.657	0.453
CSI (SW2D-DDP)	0.92	0.699	0.687	0.698	0.655	0.665	0.667	0.506
OA (SW2D)	0.94	0.852	0.847	0.855	0.843	0.848	0.853	0.866
OA (SW2D-DDP)	0.95	0.856	0.851	0.86	0.844	0.851	0.857	0.894

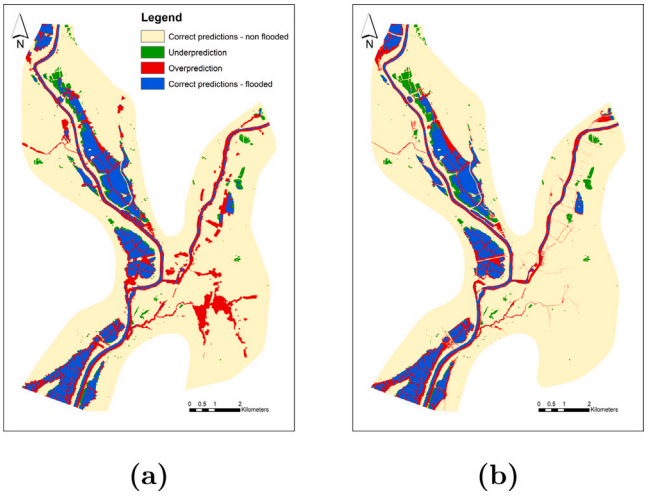

Fig. 8. Contingency maps computed from the satellite and each of the standard (a) and porosity (b) model flood maps, on December 04, 2012.

was detectable during the 2007 flood event inside Tewkesbury using a high resolution SAR backscatter image (i.e. a Terrassar-X image). As a consequence, one can argue that the absence of floodwater within Tewkesbury in the Cosmo-SkyMed images acquired in 2012 lends more weight to the SW2D-DDP flood extent map reliability.

4.2. Evaluation of simulated water level maps

Fig. 9 shows time series of root mean square deviations (RMSD) calculated between the porosity and standard model-derived water levels at a daily frequency, across the inundated areas. The corresponding time-averaged RMSDs are equal to 12.32 cm and 6.3 cm for the 2007 and the 2012 flood events respectively. The highest deviations are observed in the falling and rising limbs. During the flood, peaks are reduced and vary between 3 and 9 cm. From a practical point of view, depth deviations ranging from 10 to 15 cm in flood predictions can arguably be considered as acceptable given the vertical accuracy of the LiDAR used: ±10 cm (Sanders, 2007; Mason et al., 2003). Furthermore, boxplots are used to assess the distribution of differences between water levels simulated by the porosity and the standard models at a daily time step (Fig. 10). At first sight, it is found that the model results present a very good agreement at the flood peak since the boxplot height is very small. Positive values in the boxplots refer to higher water levels simulated by the porosity model. This is mainly observed during the rising limb and at the flood peak. This indicates that the porosity model simulates the overbanking earlier. This result is in agreement with the larger water extent simulated by the porosity model (see Figs. 6a and 7a). During the falling limb, lower values of water levels simulated by the porosity model express a larger inundation extent computed by the standard model, as obtained in (Figs. 6c and 7c).

Table 2
RMSDs computed between the water level time series simulated by the porosity (SW2D-DDP) and standard (SW2D) models and Mythe Bridge gauge data for both flood events and Tewkesbury camera data of the 2012 flood event; RMSD: root mean square deviation.

	Mythe Bridge (2007)	Mythe Bridge (2012)	Tewkesbury (2012)
RMSD (SW2D)	0.388	0.255	0.444
RMSD (SW2D-DDP)	0.371	0.237	0.425

4.3. Evaluation of simulated water levels time series

Simulated (porosity and standard model) water level time series are first evaluated using in situ observations at the Mythe Bridge hydrometric station and second using water levels estimated from the Tewkesbury camera images. When inter-comparing the two models, the results present a very good agreement (Figs. 11a, 11b and 11c). The highest discrepancies of simulated water levels compared to the gauge observations (0.90 and 0.60 m) are reached just before the 2007 flood peak (Fig. 11a) and on the first day of the 2012 flood simulation (Fig. 11b), respectively. The evaluation further shows reduced model errors during the falling limb of the 2012 flood event where the porosity model exhibit an error of less than 5 cm approximately. This is probably related to the initial condition fixed in the simulation that is set as uniform and fits the downstream level (Deerhurst). On another note, RMSDs are slightly improved, albeit not significantly, in the porosity model (Fig. 9). Both model results are also assessed using the camera images at Tewkesbury (see location in Fig. 3). The highest discrepancies with the gauge data are found in the rising limb. They are reduced when approaching the flood peak and almost fit the model results at the falling limb. Table 2 shows the porosity and standard model scores, using the RMSD metrics computed on water level time series. The considered reference is the data observed at Mythe Bridge for the 2007 and 2012 events and at Tewkesbury for the 2012 event.

5. Discussion

As described in Section 4.2, the water depth deviations of the porosity-based model with respect to the standard SW2D model, are acceptable given the vertical accuracy of the LiDAR used (c.a. 10 cm). The average flow depth in the rivers estimated over the entirety of the flood event, is about 7 m. Generally speaking, the average errors (c.a. 6 to 12 cm) are not substantial. High errors – reaching a maximum of 25 cm – are observed in the rising and the falling limb, where the porosity model seems to fill in and evacuate faster than the standard model. On the other hand, errors with respect to the gauge/camera data reach a maximum of 60 to 90 cm respectively. Since the real bathymetry and bed-shape of the river are unknown, this potentially affects the simulation results in general, and can be further improved.

In Fig. 11, the simulated levels at Mythe Bridge are lower than the observed ones, especially during the rising limb and the flood peak. This is arguably due to the simplified representation of the bathymetry in the models and to an underestimated upstream inflow for the Severn River at Saxon's Lode under high flow conditions. Indeed, as the river burst its banks around Saxon's Lode, the floodplain starts conveying a part of the flow that is not accounted for in the corresponding model boundary condition derived from the riverstream gauging station.

In terms of flood extents, results show the porosity model fills in and drains floodplain water faster than the standard model. To better assess this behaviour, we compared both model results to a series of remote sensing derived flood maps. It was shown that, during the falling limb, the observed inundation extent is closer to the one simulated with the porosity model, especially in the areas around Tewkesbury. This faster flooding and receding dynamic in the porosity model is mainly related to its ability to represent small scale topography and drains via

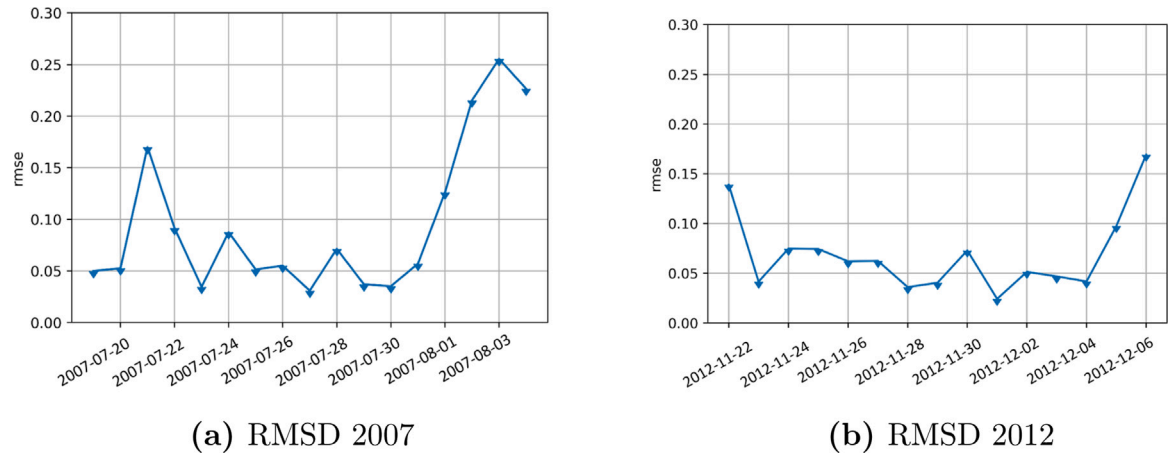

Fig. 9. Root mean square deviations (RMSD) in metres, between SW2D-DDP and SW2D simulated water level maps (resampled at DTM resolution): (a) 2007 and (b) 2012 flood events.

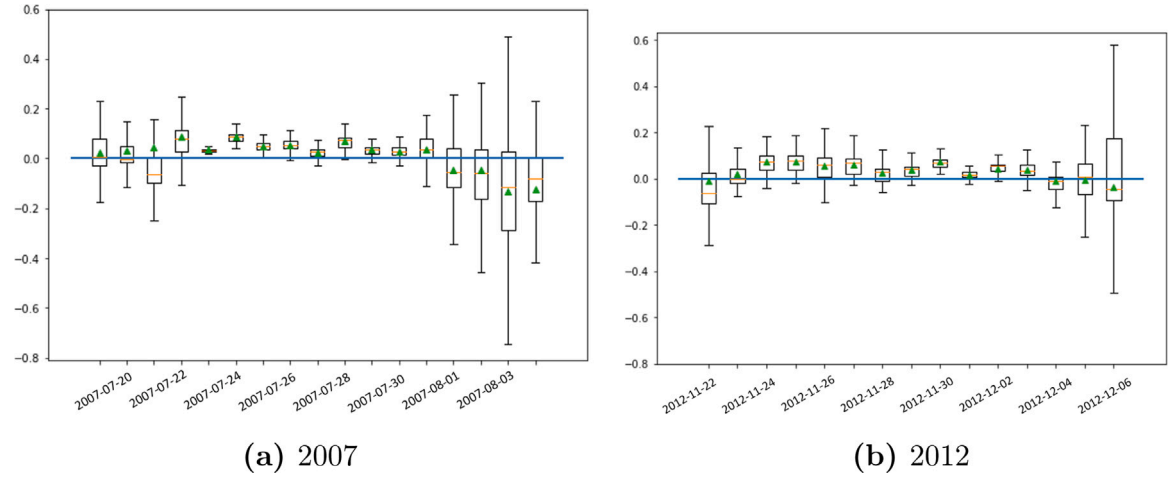

Fig. 10. Boxplots drawn from the simulated water level deviations using as a reference the standard model — orange line: median; triangle: mean; box: interquartile range; whisker ends: the lower and upper bounds: (a) 2007 and (b) 2012 flood events. (For interpretation of the references to colour in this figure legend, the reader is referred to the web version of this article.)

porosity. As mentioned in Section 2.2.1, representing small drains in the standard model requires cells with dimensions smaller than that of the drains. This means that drains should in theory be finely discretised by very small cells (Fig. 12) in the SW2D model. These drains are visible in the LiDAR topographic data (Fig. 3), but they are not captured by our standard model mesh, because the mesh cells are comparatively large. For example, the size of a cell capturing a drain would have dimensions smaller than 5 m, which would increase the number of computational cells along the drainage network. The standard mesh designed in this study consists of 29,772 cells, representing approximately 28 times more cells than that in the porosity mesh (1042 cells). Moreover, the simulation run time in that case would escalate drastically with the decrease of the simulation time step becoming inconvenient for large scale applications. Table 3 summarises the CPU times necessary for the standard and the porosity model simulations, carried out on a computer with an i7-4770 CPU processor and a memory of 16 GB RAM. For an area of 1500 km^2 and in both test cases, the CPU time required for the model simulation is 13 min vs. 3.2 days for the standard model for a 17 days flood simulation, and 12 min vs. 2.9 days for a 15 flood day event. The porosity model therefore offers the advantage of a fast model setup, while preserving high resolution data by using coarse grid cells, thus enabling reduced computational efforts. This paves the way for real time applications and long terms simulations over large areas.

All singularities and types of cross-section can be taken into account in the porosity laws as long as they are visible in the DTM. However, the spatial localisation of the singularity inside a coarse grid cell is lost, this is why it is preferable to place the interfaces on the singularities so as not to create artificial links between the cells. Since cross-sections are rarely available along the entire river and only punctual measurements are provided, a riverbed shape approximation must be made, which is facilitated by the use of porosity laws. The interpolation of river bathymetry between observed cross sections certainly has an influence on the model results, but it is the only available information. In this study we compared both models using the same bathymetric data. The linear interpolation of these profiles along the river appeared to be reasonable since no brutal variations of the slopes were observed while examining longitudinal profiles. However, further improvements are expected when having more precise bathymetry data. In this study the topography information is derived from a high resolution LiDar DTM originally at 2 m resolution and resampled at 10 m. With increasing availability of global DEMs (e.g.: SRTM 30 m at a global scale), the modelling approach can be applied in poorly gauged areas. For the specific case of urban areas, the building location map could be used to improve the DEM, based on widely available databases such as OpenStreetMap. The vegetation remains more complex to be accounted for and for the moment we may consider vegetation effects through an increased friction coefficient, as usually done in hydrodynamic modelling. In the SW2D software (classical or DDP), all parameters such as infiltration rates and friction, can be spatially distributed (e.g. based on land use maps).

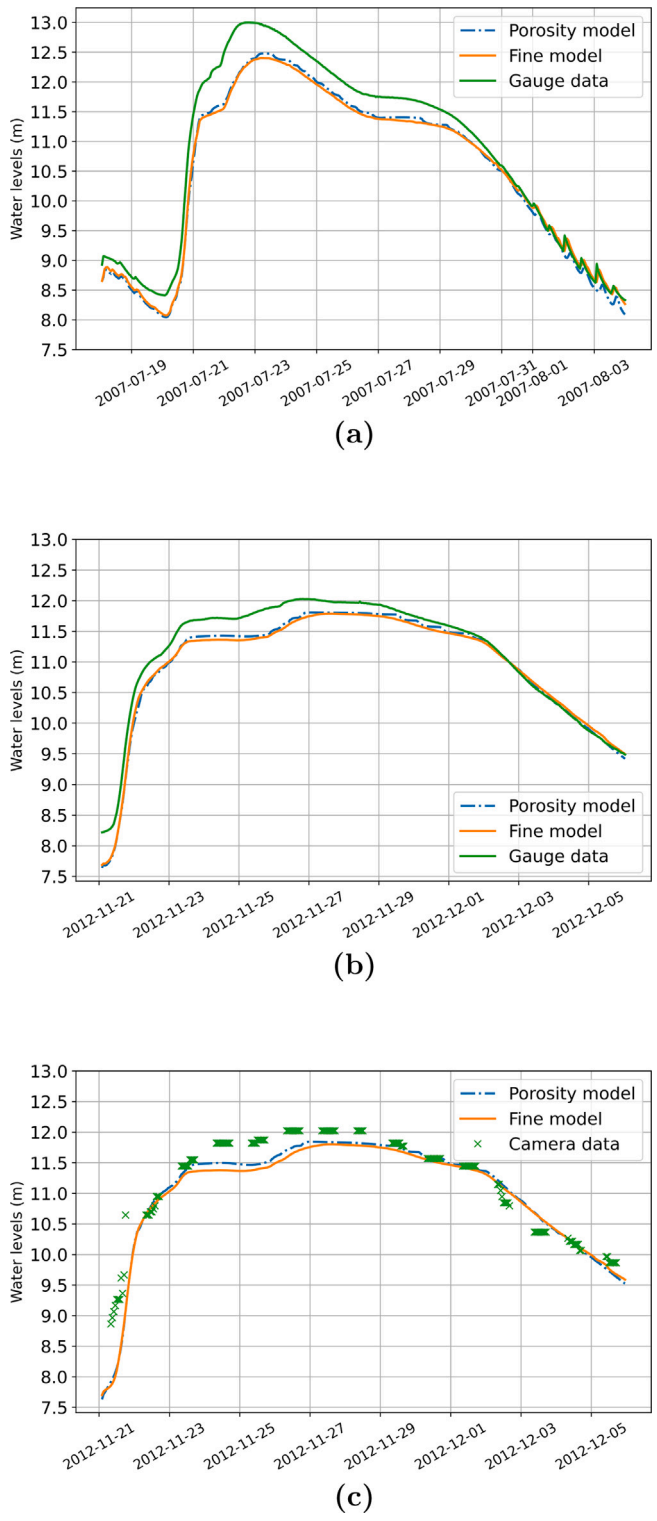

Fig. 11. Water level time series evaluation using data at Mythe Bridge for the 2007 event (a), 2012 event (b) and at Tewkesbury for the 2012 event (c).

As discussed in Guinot et al. (2018), one main limitation of the porosity modelling approach is the definition of a unique water level per computational cell, which is equivalent to considering a horizontal free surface elevation in each cell. Although the consequences of such an assumption are limited when dealing with large-scale and slow floods, they may not be negligible and should be assessed. The porosity-based approach also leads to a loss of spatial information inside coarse

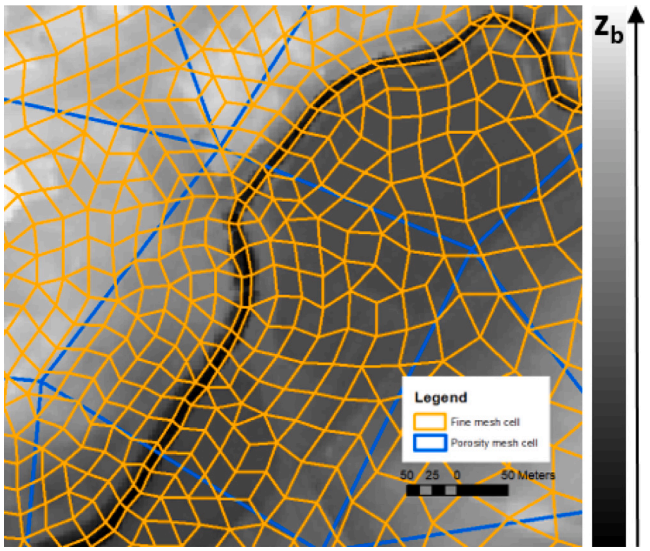

Fig. 12. Drains representation by computational cells in the SW2D (orange) and SW2D-DDP (blue) models. (For interpretation of the references to colour in this figure legend, the reader is referred to the web version of this article.)

Table 3
Simulation run time for the porosity (SW2D-DDP) and standard (SW2D) models, with the run time reduction factor.

Flood event	Simulation period	SW2D	SW2D-DDP	Reduction factor
2007	17 days	3.2 days	13 min	354 times
2012	15 days	2.9 days	12 min	348 times

grids. This can potentially create artificial links between cells unless the edges are carefully placed upon local highest points. However, one should keep in mind that this is also true for other hydrodynamic models, such as classical 2D ones. Moreover as seen before, it is possible to recover spatial information by resampling the results on the DTM as proposed in this paper, therefore preserving the original DTM data at its original resolution.

6. Conclusion

In this paper, we proposed an innovative modelling framework based on porosity to rapidly simulate flood inundations. This framework enables, for the first time, to represent both bathymetry and small-scale floodplain topography using depth-dependent porosity within comparatively large computational cells. Simulating two real test case floods over a 1500 km^2 area around the Severn and Avon confluence, has shown the following:

1. The proposed modelling approach enable to simulate flood extent maps very similar to the one simulated by the standard SW2D model with 90% agreement.
2. The evaluation based on in situ measurements indicates that the porosity model is exhibiting levels of performance comparable to and even higher than those of a standard model.
3. It is found that the porosity model is able to account for small drains within comparatively very large cells. Representing these small drains in a standard model would require very small cells, therefore leading to a much higher number of cells and a large computational demand.
4. Our experiment shows that the SW2D-DDP model simulations are c.a. 350 times faster than that of the standard model, thereby substantially reducing computational costs.

In perspective, the proposed modelling framework facilitates the retrieval of an effective bathymetry as this is represented via the porosity parameters. This opens up new perspectives for large scale applications over areas where bathymetric data are not available.

Declaration of competing interest

The authors declare that they have no known competing financial interests or personal relationships that could have appeared to influence the work reported in this paper.

Acknowledgements

This study was funded by the National Research Fund of Luxembourg through the CASCADE project (Grant no. C17/SR/11682050). The hydrometric data is provided by the UK environment agency. All authors approved the version of the manuscript to be published.

References

Arnell, N.W., Gosling, S.N., 2016. The impacts of climate change on river flood risk at the global scale. Clim. Change 134 (3), 387–401.
Baan, P.J., Klijn, F., 2004. Flood risk perception and implications for flood risk management in the netherlands. Int. J. River Basin Manage. 2 (2), 113–122.
Bates, P.D., De Roo, A., 2000. A simple raster-based model for flood inundation simulation. J. Hydrol. 236 (1–2), 54–77.
Casulli, V., 2015. A conservative semi-implicit method for coupled surface–subsurface flows in regional scale. Internat. J. Numer. Methods Fluids 79 (4), 199–214.
Chini, M., Hostache, R., Giustarini, L., Matgen, P., 2017. A hierarchical split-based approach for parametric thresholding of sar images: Flood inundation as a test case. IEEE Trans. Geosci. Remote Sens. 55 (12), 6975–6988.
Chini, M., Pelich, R., Pulvirenti, L., Pierdicca, N., Hostache, R., Matgen, P., 2019. Sentinel-1 insar coherence to detect floodwater in urban areas: Houston and hurricane harvey as a test case. Remote Sens. 11 (2), 107.
Cunge, J., 1980. Practical Aspects of Computational River Hydraulics. Pitman Publishing Ltd., London,(17 CUN), p. 420, 1980.
Defina, A., 2000. Two-dimensional shallow flow equations for partially dry areas. Water Resour. Res. 36 (11), 3251–3264.
Defina, A., D'alpaos, L., Matticchio, B., 1994. A new set of equations for very shallow water and partially dry areas suitable to 2d numerical models. In: Modelling of Flood Propagation over Initially Dry Areas. ASCE, pp. 72–81.
Delenne, C., Bailly, J.-S., Rousseau, A., Hostache, R., Boutron, O., 2021. Endorheic waterbodies delineation from remote sensing as a tool for immersed surface topography. IEEE Geosci. Remote Sens. Lett..
Durand, M., Neal, J., Rodríguez, E., Andreadis, K.M., Smith, L.C., Yoon, Y., 2014. Estimating reach-averaged discharge for the river severn from measurements of river water surface elevation and slope. J. Hydrol. 511, 92–104.
Finaud-Guyot, P., Delenne, C., Guinot, V., Llovel, C., 2011. 1D–2d coupling for river flow modeling. C. R. Méc. 339 (4), 226–234.
Giustarini, L., Hostache, R., Matgen, P., Schumann, G.J.-P., Bates, P.D., Mason, D.C., 2012. A change detection approach to flood mapping in urban areas using terrasar-x. IEEE Trans. Geosci. Remote Sens. 51 (4), 2417–2430.
Guinot, V., 2012. Multiple porosity shallow water models for macroscopic modelling of urban floods. Adv. Water Resour. 37, 40–72.
Guinot, V., Delenne, C., Rousseau, A., Boutron, O., 2018. Flux closures and source term models for shallow water models with depth-dependent integral porosity. Adv. Water Resour. 122, 1–26.
Guinot, V., Sanders, B.F., Schubert, J.E., 2017. Dual integral porosity shallow water model for urban flood modelling. Adv. Water Resour. 103, 16–31.
Guinot, V., Soares-Frazão, S., 2006. Flux and source term discretization in two-dimensional shallow water models with porosity on unstructured grids. Internat. J. Numer. Methods Fluids 50 (3), 309–345.
Hervouet, J.-M., Samie, R., Moreau, B., 2002. Modelling urban areas in dam-break flood-wave numerical simulations. Dev. Water Sci. 47, 1613–1620.
Hostache, R., Chini, M., Giustarini, L., Neal, J., Kavetski, D., Wood, M., Corato, G., Pelich, R.-M., Matgen, P., 2018. Near-real-time assimilation of sar-derived flood maps for improving flood forecasts. Water Resour. Res. 54 (8), 5516–5535.
Hostache, R., Matgen, P., Giustarini, L., Teferle, F.N., Tailliez, C., Iffly, J.-F., Corato, G., 2015. A drifting GPS buoy for retrieving effective riverbed bathymetry. J. Hydrol. 520, 397–406.
Inria Lemon Team, last access 2022. SW2D Software: http://sw2d.inria.fr/.
Kim, B., Sanders, B.F., Famiglietti, J.S., Guinot, V., 2015. Urban flood modeling with porous shallow-water equations: A case study of model errors in the presence of anisotropic porosity. J. Hydrol. 523, 680–692.
Larnier, K., Monnier, J., Garambois, P.-A., Verley, J., 2021. River discharge and bathymetry estimation from swot altimetry measurements. Inverse Probl. Sci. Eng. 29 (6), 759–789.
Mason, D.C., Cobby, D.M., Horritt, M.S., Bates, P.D., 2003. Floodplain friction parameterization in two-dimensional river flood models using vegetation heights derived from airborne scanning laser altimetry. Hydrol. Process. 17 (9), 1711–1732.
Meyer, V., Scheuer, S., Haase, D., 2009. A multicriteria approach for flood risk mapping exemplified at the mulde river, Germany. Nat. Hazards 48 (1), 17–39.
Neal, J., Schumann, G., Bates, P., 2012. A subgrid channel model for simulating river hydraulics and floodplain inundation over large and data sparse areas. Water Resour. Res. 48 (11).
Oubanas, H., Gejadze, I., Malaterre, P.-O., Durand, M., Wei, R., Frasson, R.P., Domeneghetti, A., 2018. Discharge estimation in ungauged basins through variational data assimilation: The potential of the swot mission. Water Resour. Res. 54 (3), 2405–2423.
Pradhan, B., Hagemann, U., Tehrany, M.S., Prechtel, N., 2014. An easy to use arcmap based texture analysis program for extraction of flooded areas from terrasar-x satellite image. Comput. Geosci. 63, 34–43.
Revilla-Romero, B., Wanders, N., Burek, P., Salamon, P., de Roo, A., 2016. Integrating remotely sensed surface water extent into continental scale hydrology. J. Hydrol. 543, 659–670.
Sanders, B.F., 2007. Evaluation of on-line dems for flood inundation modeling. Adv. Water Resour. 30 (8), 1831–1843.
Sanders, B.F., Schubert, J.E., Gallegos, H.A., 2008. Integral formulation of shallow-water equations with anisotropic porosity for urban flood modeling. J. Hydrol. 362 (1–2), 19–38.
Schaefer, J.T., 1990. The critical success index as an indicator of warning skill. Weather Forecast. 5 (4), 570–575.
Soares-Frazão, S., Lhomme, J., Guinot, V., Zech, Y., 2008. Two-dimensional shallow-water model with porosity for urban flood modelling. J. Hydraul. Res. 46 (1), 45–64.
Tehrany, M.S., Pradhan, B., Jebur, M.N., 2014. Flood susceptibility mapping using a novel ensemble weights-of-evidence and support vector machine models in gis. J. Hydrol. 512, 332–343.
Vetra-Carvalho, S., Dance, S.L., Mason, D.C., Waller, J.A., Cooper, E.S., Smith, P.J., Tabeart, J.M., 2020. Collection and extraction of water level information from a digital river camera image dataset. Data Brief 33, 106338.
Willems, P., Vaes, G., Popa, D., Timbe, L., Berlamont, J., 2002. Quasi 2d river flood modelling. In: River Flow, Vool. 2. Swets & Zeitlinger Lisse, pp. 1253–1259.
Wood, M., Hostache, R., Neal, J., Wagener, T., Giustarini, L., Chini, M., Corato, G., Matgen, P., Bates, P., 2016. Calibration of channel depth and friction parameters in the LISFLOOD-fp hydraulic model using medium-resolution SAR data and identifiability techniques. Hydrol. Earth Syst. Sci. 20 (12), 4983–4997.
Yoon, Y., Durand, M., Merry, C.J., Clark, E.A., Andreadis, K.M., Alsdorf, D.E., 2012. Estimating river bathymetry from data assimilation of synthetic swot measurements. J. Hydrol. 464, 363–375.
Zhang, W., Zhang, X., Liu, Y., Tang, W., Xu, J., Fu, Z., 2020. Assessment of flood inundation by coupled 1d/2d hydrodynamic modeling: A case study in mountainous watersheds along the coast of southeast China. Water 12 (3), 822.